Energy Harvesting and Buffering for Cyber Physical Systems: A Review

Grayson Honan, Nicholas Gekakis, Moeen Hassanalieragh, Andrew Nadeau, Gaurav Sharma, Tolga Soyata
Dept. of Electrical and Computer Engineering, University of Rochester

ABSTRACT

Cyber-Physical Systems (CPS) enable data processing in the field. By keeping the processing unit in close proximity to the data-acquisition point, latency can be reduced and the impact of limited communication bandwidth and power availability can be mitigated. To work autonomously for extended periods of time without requiring user support, CPS must harvest energy from sources such as solar radiation, ambient RF, wind, rain, or vibrations. Additionally, the energy harvested by CPS needs to be buffered because of the uncertain availability of harvested sources. The two primary buffering mechanisms are batteries and supercapacitors, with the batteries being further classified into their own sub-categories. This chapter reviews existing energy sources for CPS and compares/contrasts these sources. Based on the characteristics of the different sources, conclusions are drawn as to which sources are apt for what type of environments.

Keywords: Energy harvesting; Energy buffering; Supercapacitors; Cyber-physical Systems

INTRODUCTION

Cyber-Physical Systems (CPS) rely on generating their own energy to operate autonomously in the field without requiring maintenance. Solar, RF, wind, and vibration energy are among the sources that have been used or proposed for powering CPS. Each of these sources comes with its own advantages and disadvantages. For example, while ambient RF energy can be harvested in the dark, or where no solar energy is available, it requires a large area for the antenna, which could make CPS impractical. Alternatively, solar energy can provide the largest power output, however, it is only available in areas where there is consistent sunshine (Chalasani & Conrad, 2008). Wind energy is widely available, but it requires a mechanical transmission which can be expensive to maintain; wind also tends to be extremely variable in terms of strength. Therefore, the optimal choice for energy harvesting is not obvious and requires detailed analysis of the location and operation modes of the CPS. After harvesting, energy must be buffered using a storage device to provide power for the CPS operations during time periods where the energy source is unavailable. For example, in equatorial regions where sunlight cycles on and off on a 12 hour cycle, the energy buffer can provide the operational power during dark hours. Combining different energy sources (e.g., solar and RF) can reduce the demands on the buffering, but cannot completely eliminate the need for buffering. Therefore, different mechanisms for buffering must be carefully considered before deploying a CPS. Options for buffering include rechargeable batteries, such as Li-Ion, lead-acid, NiCd, and Ni-Mh, or supercapacitors. While supercapacitors are virtually maintenance-free, for CPS with moderate to large power requirements, they take up a large amount of space posing a challenge for CPS deployment (Buchmann, 2011). Batteries can solve the energy density problem, at the expense of three- to four-year maintenance cycles (as compared to 10-year cycles for supercapacitors). This chapter provides a review of existing energy sources and energy buffering mechanisms and compares each option.

ENERGY SOURCES

Today, solar energy harvesting using photovoltaic cells is the mainstream energy harvesting technology for CPS. However, other sources of energy exist that may be better suited for harvesting in particular environments. In situations where solar needs to be supplemented, or cannot be used at all, radio frequency, wind, or vibration energy harvesting systems can be utilized. In this section we provide an overview of each harvesting technology and conclude with an analysis that identifies which technology is best suited to a given environment.

Harvesting technology	**Power density**
Solar	
Solar cells (outdoors at noon)	15 mW/cm^2
Radio Frequency	
Dedicated source at short range	50 $\mu W/cm^2$
Ambient RF	2 $\mu W/cm^2$
Wind	
Small-scale turbine	83.3 $\mu W/cm^3$
Vibration	
Piezoelectric (shoe inserts)	330 $\mu W/cm^3$
Vibration (Magnetostrictive Metglas material)	606 $\mu W/cm^3$

Table 1. Footprint area densities of common energy harvesting technologies (Wang & Yuan, 2007).

Solar

Photovoltaic (PV) cells are devices that convert light energy to electrical energy; they're used in applications ranging from low-power devices to large scale harvesting for homes and commercial buildings.

The most common choice for PV materials is a silicon-based cell. These devices offers a reasonable price to performance ratio and represent a relatively mature technology, with the installation price per watt dropping 5-7% annually for the past decade (Feldman, Barbose, Margolis, Darghouth, & Goodrich, 2012). There are three main categories for silicon-based PV cells: monocrystalline (mono-Si or single-crystal-Si), amorphous (a-Si), and polycrystalline (mc-Si or p-Si) (Green, Emergy, Hishikawa, Warta, & Dunlop, 2014). Monocrystalline silicon is the most expensive of the three, but typically reaches efficiencies of around 25% (Green, Emergy, Hishikawa, Warta, & Dunlop, 2014). Polycrystalline types are cheaper than monocrystalline, but only reach around 20% efficiency (Green, Emergy, Hishikawa, Warta, & Dunlop, 2014). Amorphous silicon is the cheapest of these three categories, and is used regularly in lower power devices such as simple four-function calculators. In a typical outdoor environment, amorphous cells can reach efficiencies of around 10%, but indoors can maintain an efficiency between 3 and 7% where monocrystalline variants can only reach 1-2% efficiency while indoors (Hande, Polk, Walker, & Bhatia, 2007). Amorphous cells are well-suited to absorb indoor light spectra, but other cell types are less efficient at converting the low intensity of artificial light into electricity (Randall & Jacot, 2002). The vast majority of PV systems are installed outdoors, where a square meter of harvesting space can yield between 100 and 1000 W; but for indoor systems, on the other hand, about 10 W/m^2 can be expected (Hande, Polk, Walker, & Bhatia, 2007).

Figure 1. Monocrystalline cells (left) have a distinctive rounded geometric shape and appear smooth, while polycrystalline cells (right) are rectangular with a jagged internal structure. (DebbieMous, 2011; Andrewatla, 2007)

Wireless sensor networks are the major focus of research in low power solar energy harvesting, with applications in medicine, environmental monitoring, and military operations. The Smart Dust program at the University of California, Berkeley was one of the first major investigations into the use of photovoltaic cells in wireless sensor networks. The Smart Dust program used the energy harvested from PV panels to communicate optically with a laser-based transceiver system (Kahn, Katz, & Pister, 2000; Atwood, Warneke, & Pister, 2000).

The power needs of a given CPS installation dictate the size of PV panel needed. The power density for solar cells harvesting outdoors at noon is approximately 15 mW/cm^2 (Chalasani & Conrad, 2008). Based on this information, an appropriately-sized panel can be selected. Because the thickness of PV panels is negligible in most applications, PV panel power density is typically considered in terms of power-per-area rather than per-volume. For low power PV panels (around 1 W), the thickness is around 4 mm or less. Larger panels (around 250 W) have a thickness of approximately 4.5 cm. At the time of writing, the cost of consumer PV panels in the 1 to 3 W range is around $10 and 5 to 10 W PV panels cost around $30.

Overall, solar energy harvesting is a very strong option for CPS and is extremely effective in comparison to other harvesting methods provided that the environment has sunlight available. The efficacy of PV

panels is obviously very dependent on the location's light availability. The quality of a light source can be thought of in terms of intensity (typically, measured in lumens) and interruptions. For outdoor environments, intensity is determined by the angle of incidence for the sunlight on the panel and the thickness of the atmosphere traversed. This makes areas that are further from the equator less likely candidates for solar energy harvesting. Interruptions are the second factor we consider in the quality of a light source. When the sun is the light source, intermittent cloud coverage and nightfall are primary causes of interruptions. For artificial light, the lifetime of the bulb and the efficiency of the solar panel within the emitted spectral bands from the bulb need to be considered. Regardless of the light source being used, one also needs to consider the possibility of dust or other debris blocking light from efficiently entering the PV cells.

In addition to light source quality, one also needs to consider the solar panels ability to harvest solar energy. As explained above, indoor situations call for amorphous PV panels since they maintain a higher efficiency (Hande, Polk, Walker, & Bhatia, 2007). And in outdoor situations, monocrystalline has ~25% efficiency, polycrystalline has ~20% efficiency and amorphous has around 10%. Installations of PV panels may also include the ability to automatically adjust their orientation to track the light source and harvest more energy than static installations.

Radio Frequency

Radio Frequency (RF) energy harvesting is an attractive method for powering wireless devices that range from consumer electronics, such as mobile phones, to sensor nodes used by researchers to collect data in remote environments. The utility of RF harvesting comes from the fact that energy in this form is readily available, consistent, and reliable when compared to energy harvesting from other environmental sources such as solar radiation, wind, or vibrations.

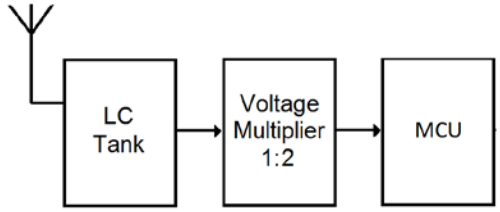

Figure 2. A block diagram for a standard RF energy harvester.

The most important apparatus in harvesting RF signals is the rectenna, a combination of rectifier circuitry, most often in the form of either one Schottky diode or several cascaded Schottky diodes, and an antenna, most often a dipole antenna (Visser & Vullers, 2013). When in the presence of a suitable RF signal, i.e., electromagnetic waves within an appropriate frequency band, a voltage is induced in the antenna as an alternating current (AC) signal. The rectifier circuitry then converts the signal to direct current (DC), which can then be used to drive a target device. In addition to the rectifier and antenna, the rectenna will frequently also include some form of DC to DC converter because, in the majority of cases, the output voltage of the rectifying circuitry will be too low to be utilized directly in an application (Jabbar, Song, & Jeong, 2010).

The downside to RF harvesting is that the area density of recoverable energy is very low, reaching at most 50 $\mu W/cm^2$ (Roundy, Steingart, Frechette, Wright, & Rabaey, 2004). This low power yield is a result of the relative low density of ambient RF energy in most locations and inefficiencies in the antennas used during energy harvesting (Hudak & Amatucci, 2008). In ideal conditions, the antennas used during energy harvesting only reach a maximum of 45% efficiency (Hudak & Amatucci, 2008). One method to increase the energy harvested from RF signals is to use a dedicated RF source, rather than harvesting energy from ambient RF signals. A dedicated source can offer higher energy density because of its close

proximity to the device (Visser & Vullers, 2013). In the context of CPS, this solution loses some key advantages over ambient RF energy harvesting because the dedicated source needs its own energy supply. Such a system would also require the harvester to stay within close proximity of the dedicated RF source. Due to the low power yield of ambient RF harvesting, dedicated RF harvesting is the more widely used method, with its main applications in Radio Frequency Identification (RFID) (Hudak & Amatucci, 2008).

In RFID, a small device stores identifying data and remains powered off until it needs to be read. During a read, radiofrequency is emitted to power on the RFID device. The RFID device can then send its data for reading through one of several backscattering methods. When the reading device ceases transmitting its RF signal, the RFID device powers off once again (Curty, Joehl, Dehollain, & Declercq, 2005). This is not strictly considered energy harvesting because the energy gathered is used to directly power the RFID devices rather than to charge a battery (Hudak & Amatucci, 2008). It is also important to note that RFID devices are not a form of CPS because, on their own, they do no computational tasks.

Another challenge in RF energy harvesting is impedance matching. Because RF signals exhibit variable frequency (ambient RF frequencies typically range from 1GHz to 3.5 GHz), the impedance of the circuit needs to be adjusted to continuously ensure maximum power (Shameli, Safarian, Rofougaran, Rofougaran, & De Flaviis, 2007). Currently, most research on RF energy harvesting efficiency is focused on improving the antennas that gather the RF signals (Thomas, Qidawi, & Kellogg, 2006). One breakthrough in improving the space efficiency of RF antennas showed that four antennas can be placed in the area that would normally be occupied by just two (Mi, Mickle, Capelli, & Swift, 2005).

One of the great advantages of RF energy harvesting is that the system can be made very small; typically, the greatest amount of area is being used by the antenna itself. Usually, an RFID device will only be slightly larger than a grain of rice, and this includes circuitry for the data storage and transmission (Foster & Jaeger, 2007). If more power is required, the antenna must be made larger, but usually RF energy harvesting systems occupy at most few square inches (Hudak & Amatucci, 2008).

The major disadvantage of RF energy harvesting is its low power yield; in order to get a power yield on the order of solar panels, a very large antenna would be needed. When using a dedicated RF supply at close range, 50 $\mu W/m^2$ can be harvested. If ambient RF signals are being used, only about 2 $\mu W/m^2$ can be harvested (Visser & Vullers, 2013).

RF harvesting devices require very little maintenance because no moving parts are involved and because they don't need to be exposed to the environment, unlike a solar or wind harvester.

If a dedicated RF supply is being used, RF energy harvesting can be done virtually anywhere; however due to its low power yield, RF harvesting should not be considered if access to direct sunlight is available. If the device relies on ambient RF waves, then an urban environment would yield far greater power than other locations.

Figure 3. A wind energy harvester at the University of Rochester.

Wind

Wind energy harvesting exploits the mechanical energy of blades or cups of a windmill spun by ambient wind, which is converted into electrical energy via a generator (Goudarzi & Zhu, 2013). Modern wind

turbines are capable of providing power on the order of 2.5 MW or more in favorable wind conditions (Goudarzi & Zhu, 2013). When scaled down to very small sizes, generators cease to be practical in converting the mechanical energy harvested from the wind into electrical energy. This is because when the cross sectional area of the wind turbine's blades are very small (2-5 in^2), the force created is on the order of 0.1 N or less under typical wind speeds that range between 3 and 10 mph. This is not enough force to efficiently operate a generator (Myers, Vickers, Kim, & Priya, 2007). Power per area can be increased by equipping the harvester with a diffuser (Ohya, Karasudani, Sakurai, Abe, & Inoue, 2008); however, to achieve the greatest efficiency at the smallest possible scale, a different method of energy conversion is required.

By replacing the usual generator found within a wind harvesting device with bimorph piezoelectric transducers, researchers from the University of Texas at Arlington created a successful small-scale wind energy harvesting device (Myers, Vickers, Kim, & Priya, 2007). When subjected to mechanical stress, piezoelectric transducers generate a voltage difference between two electrodes, thereby converting mechanical energy into electrical energy (Myers, Vickers, Kim, & Priya, 2007). Instead of using the rotational energy provided by a wind turbine to spin a conductor in a magnetic field, the rotational energy is used to spin a shaft with stoppers fixed on one end. As the shaft turns, the stoppers strike the piezoelectric transducers that are evenly spaced around the shaft, just within reach of the stoppers. The mechanical stress introduced when a stopper hits one of the transducers creates a voltage difference in the transducer, which can then be used to power a load. After optimizing the design for metrics such as space efficiency, minimizing damage done to the transducers, and synchronizing the stress put on the individual transducers this new design yielded 5 mW of continuous power when operating in average wind speeds of 10 mph. This design used 18 piezoelectric bimorph transducers, but more transducers can be used to generate more power. If more transducers are added to the design, stronger winds are required (Myers, Vickers, Kim, & Priya, 2007).

One drawback for wind harvesting, especially for cyber physical systems, is that the space required for wind energy harvesting is quite large relative to other forms of energy harvesting. This is because a large cross sectional area is needed to capture the wind's energy, and because the mechanism used to convert the energy, either an electric generator or piezoelectric transducers, requires its own casing. Additionally, because wind harvesting systems use many moving parts, maintenance is typically necessary over the lifetime of the harvester to deal with the mechanical wear and tear.

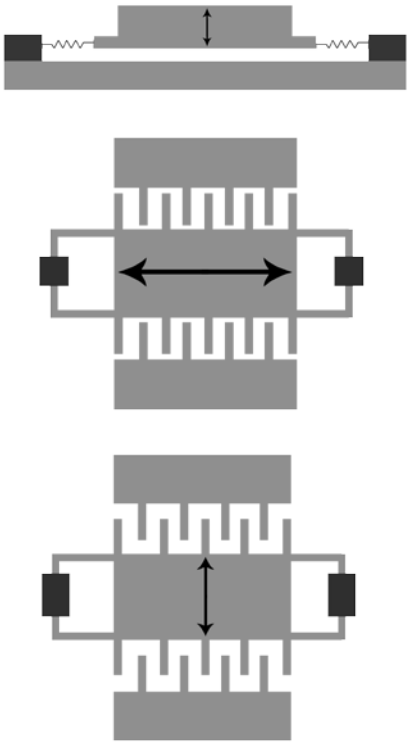

Figure 4. Out-of-plane gap closing type (top); In-plane gap closing type (middle); In-plane overlap type (bottom) Based on Shad, Wright, & Pister, 2002.

Vibration

Vibration energy can be harvested from a variety of sources including raindrop impacts, industrial machinery, transport such as subways and cars, low-frequency seismic activity, and human motion (Guigon, Chaillout, Jager, & Despesse, 2008b). Research into

ambient vibration energy harvesting can be classified into three main categories: smart material, electromagnetic, and electrostatic generation (Beeby, Tudor, & White, 2006; Wang & Yuan, 2007). Smart materials can be further classified into the categories of piezoelectric and magnetostrictive materials (Wang & Yuan, 2007). Piezoelectric materials are much more common, but magnetostrictive materials are an emerging candidate for energy harvesting applications. Mechanical deformation of a piezoelectric material typically produces power on the order of microwatts, as does the mechanical deformation of a magnetostrictive material while possibly yielding higher average power and power density (Beeby, Tudor, & White, 2006; Wang & Yuan, 2007). The efficacy of piezoelectric generators relies heavily on the type of piezoelectric material being used, the shape and size of the selected material, and the material's orientation in relation to the mechanical forces that are deforming it (anisotropy) (Beeby, Tudor, & White, 2006). As with all transduction techniques, the efficiency with which mechanical energy is converted into electrical energy relies strongly on the apparatus being used to capture the mechanical energy, and its potential strengths or weaknesses in effectively translating mechanical energy in a given axis of motion (Chalasani & Conrad, 2008).

Piezoelectric generators are simple to implement in MEMs, but are fragile and can allow leakage of charge. Magnetostrictive materials are difficult to implement in MEMS, but don't suffer from the depolarization or charge leakage problems that piezoelectric generators face (Wang & Yuan, 2007).

Electromagnetic generators work on the principle of electromagnetic induction. A spring-mass system, where the magnetic mass provides changing magnetic flux in the presence of a conductor coil produces microwatts of power on average (Beeby, Tudor, & White, 2006). Relative to other vibration-driven generators, electromagnetic generators are large and difficult to implement in MEMS (Chalasani & Conrad, 2008). The main disadvantages of electromagnetic generators include their size and low peak voltage of only around 0.1V; smart materials and electrostatic generators have voltages of 2~10V (Wang & Yuan, 2007).

Electrostatic generators harvest energy using charged capacitor plates moving back and forth relative to each other, oscillating between minimum capacitance and maximum capacitance (Beeby, Tudor, & White, 2006). As the capacitance oscillates with constant charge on the plates, the voltage on the plates varies inversely with the distance between the plates (Shad, Wright, & Pister, 2002). According to Beeby, Tudor, and White (2006), the work done by vibrations "against the electrostatic force between the plates provides the harvested energy" (p. R187). There are three types of electrostatic generators - each one characterized by its unique structure and orientation of capacitor plates (Shad, Wright, & Pister, 2002). As illustrated in Figure 4, out-of-plane gap closing electrostatic generators work with two

	Electromagnetic (mm^3)	Electrostatic (mm^3)	Piezoelectric (mm^3)
	5.4	75	16000
	240	750	214
	2100	1000	25000
	840	800	125
	30000	1800	1000
	4	32.4	1000
	2000		1947
	250		60
	1000		2185
	1000		2
	9000		0.9
			0.0027
Average	4222	743	3961

Table 2. Volume of vibration energy harvesting devices (Beeby, Tudor, & White, 2006).

relatively large capacitive plates separated by a gap that closes due to vibrations perpendicular to the plates. In order for this generator to produce large capacitance changes, and thus be effective, the gap between the plates must become very small (Shad, Wright, & Pister, 2002). As Shad, Wright, and Pister explain, this type is also prone to shorting due to the plates becoming permanently stuck together via surface interaction forces, and thus this is a less desirable design. The second type of electrostatic generator is the in-plane gap closing method. The capacitive plates in this design are finger-like projections interwoven with capacitive plates extending from the moving part of the design (Shad, Wright, & Pister, 2002). As the apparatus vibrates in-plane with the movable section of the devices, the fingers get closer together and further apart, but the overlap remains the same. In-plane gap closing designs can easily incorporate mechanical stops to prevent shorts, so this design doesn't suffer from the problems of out-of-plate gap closing generators (Shad, Wright, & Pister, 2002). Finally, in-plane overlap varying electrostatic generators work with a similar, interwoven finger design, but rather than varying the gap between the plates, vibrations in this scheme change the overlap area of the fingers (Shad, Wright, & Pister, 2002).

Electrostatic devices are easily implemented in MEMS and don't need a smart material, although they do require an additional voltage source to provide the initial charge to the capacitive plates (Wang & Yuan, 2007).

As shown in Table 2, Beeby et al's survey on vibration energy harvesting indicates the average electromagnetic device is approximately 4220 mm^3, the average piezoelectric device is approximately 3960 mm^3, and the average electrostatic device is approximately 740 mm^3 (Beeby, Tudor, & White, 2006).

Vibration energy typically produces power on the order of microwatts, although power on the order of milliwatts can be harvested in extreme conditions. Raindrop impacts for example may be capable of producing 12 milliwatts in downpour conditions with large size drops (Guigon, Chaillout, Jager, & Despesee, 2008a).

Electrostatic, electromagnetic and piezoelectric vibration energy harvesters were the subject of Beeby et al's survey. Table 3 shows the power generation capability of the various devices surveyed. Note that magneticstrictive materials were not part of Beeby's survey, most likely due to the few number of papers on the subject in the context of energy harvesting.

Vibration energy harvesting devices are generally reliable and easy to maintain. Electromagnetic devices, in particular, are quite reliable as there is very little chance for physical contact between the moving and stationary parts of the device, which could cause a short or physical damage to the device (Chalasani & Conrad, 2008).

Electromagnetic ($\mu W/mm^3$)	Electrostatic ($\mu W/mm^3$)	Piezoelectric ($\mu W/mm^3$)
0.056	0.8533	0.08125
2.21	0.0049	0.08879
0.00000019	0.11	0.336
0.214	0.0075	0.0168
0.1333	0.5844	0.21
0.625	2.16	0.375
0.000002		0.006112
0.00576		0.0000167
0.01		0.03661
0.83		0.05
0.7778		0.67
		37

Table 3. Power generated per mm^3 for vibration energy harvesting devices (Beeby, Tudor, & White, 2006).

Piezoelectricity is a suitable transduction method in areas where there is a consistent, significant source of vibration. Other energy harvesting techniques can produce more power, such as solar harvesting, but if sunlight isn't present or is unreliable, vibration converters can provide the energy for low power embedded CPS. Some suitable sources for vibration energy harvesting include train tracks, automobile engines, cardiac tissue, geological fault lines, raindrop impacts, areas of high foot traffic, and factory machinery.

ENERGY BUFFERING

In order to investigate energy buffering, it's important to be familiar with how batteries and supercapacitors are rated in terms of capacity and energy. The capacity of energy buffers is expressed in ampere-hours (Ah), or frequently milliampere-hours (mAh). This is equal to the amount of charge transferred at a steady current over one hour. In order to accurately calculate energy, one needs to integrate the power delivered over the discharge interval. In slowly discharging batteries, voltages tend to linearly decrease as they drain, so the energy of a battery can be easily estimated by assuming a constant average voltage.

$$\textbf{Energy (J)} \approx \textbf{Average Voltage (V)} * \textbf{Capacity (Ah)} * 3600 \frac{\textbf{s}}{\textbf{h}}$$

Battery energy can also be thought of in terms of kilowatt-hours. Assuming constant power, a kilowatt-hour measures the total energy consumed in one hour.

$$kW * h = kW * 3600\ s = \frac{kJ}{s} * 3600\ s = 3600\ kJ$$

BATTERIES

Lead-Acid

Lead-acid batteries are the oldest form of rechargeable batteries and have maintained their position as the most widely used rechargeable battery for over one hundred years. This is true despite their relatively small storage capacity thanks to their dominance in the automotive market, where they provide cars with the energy required for lighting, and ignition functions associated with starting (Kularatna, 2011).

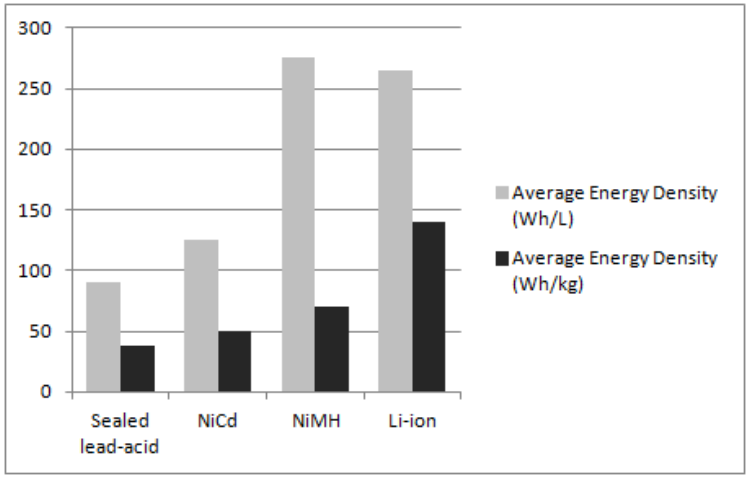

Figure 5. A comparison of common rechargeable battery types in terms of both volumetric and gravimetric energy density (Kularatna, 2011).

Lead-acid batteries are manufactured with capabilities ranging from less than 1 Ah to greater than 3000 Ah (Bullock, 1994). At 25˚C, the standard cell potential is 2.048 V and common lead-acid batteries are capable of supplying between 30 and 55 Wh/kg (Bullock, 1994). Normally, the

battery's capacity will remain very near its expected voltage for most of its life, and then will eventually lose some capacity due to age and usage (Kularatna, 2011). Lead-acid batteries are also highly versatile: different lead-acid battery designs have achieved up to a 70-year float life, more than 1000 deep-discharge cycles, power of up to 200 W/kg, and have been made with as little 6mm thickness (Bullock, 1994).

Lead-acid batteries are categorized both by the type of electrode they use as well as their electrolyte configuration. There are three electrode types: Planté, Fauré or pasted, and tubular (Bullock, 1994; Kularatna, 2011). The Planté electrodes consist of high surface area plates that have been corroded in acid to form lead dioxide on the surface. They are used exclusively for industrial applications in which long life is prioritized over high specific energy (Bullock, 1994).

Fauré plates are made by applying a lead paste to a lead grid. Due to the softness of pure lead, a lead alloy is often used to prevent deformation of the plates; antimony has historically been added to prevent grid growth, but antimony accelerates water loss. Lead-calcium alloys are a suitable replacement for antimony, as they can be used to prevent grid corrosion and don't cause water loss. High quality lead-calcium Fauré electrodes are very low maintenance and do not require water replacement throughout the lifetime of the battery (Bullock, 1994). The paste applied to Fauré electrodes consists of powdered lead oxide, sulfuric acid, and water. It gets applied to the grid at a high temperature and humidity to form a hardened porous structure. Fauré electrodes are excellent when low cost or high specific energy or power is required.

Rechargable Battery Type	Typical cell voltage (Volts)	Average life cycles (Cycles)	Average self discharge rate (%/month)
Sealed lead-acid	2.0	1250	3%
NiCd	1.2	750	20%
NiMH	1.2	650	23%
Li-ion	3.6	1100	8%

Table 4. A comparison of common rechargeable battery types in terms of cell voltage, life cycles, and self discharge rate (Kularatna, 2011).

Tubular electrodes are made by packing lead oxide powder into porous tubes made of chemically inert fibers; lead rods are then inserted down the center of each tube and connected together in parallel. In general, tubular electrodes can only be used as the positive electrode and are used in combination with a negative Fauré electrode; they make up for their lack of versatility by having very high deep cycle life.

Two types of electrolytes are used in lead acid batteries: flooded and Valve Regulated Lead-Acid (VRLA) (Bullock, 1994). VRLAs can be further broken down into gelled and separated implementations. In a flooded lead-acid battery, the entire system is flooded with 30-40% sulfuric acid; however, this design requires regular maintenance. When a flooded lead-acid battery reaches 85-90% of its charge capacity, the recharge reaction becomes less efficient and water starts to break down into hydrogen and oxygen gas. Because of this, the batteries cannot be sealed, or pressure will start to accumulate. As this water is lost as gas over time, water needs to be re-added to the system.

VRLA batteries were designed to minimize the problem of water loss by focusing on a design that that promotes the chemical recombination of oxygen at the negative electrode (Bullock, 1994). Some VRLA designs achieve up to 99% oxygen recombination efficiencies. The remaining gas that does not get reconverted to water is vented out via a one way pressure relief vent, which leads to the names for this

design, Valve Regulated Lead-Acid (VRLA) or Sealed Lead-Acid (SLA).

There are two kinds of VRLA batteries: the gelled electrolyte and the retained (or absorbed) system. In the gelled electrolyte system, the electrolyte is suspended in a silica gel; in the retained system, a glass fiber separator absorbs and retains the liquid electrolyte (Kularatna, 2011). While the automotive industry still primarily employs the basic flooded type of Lead-Acid battery, newer VRLA batteries are becoming popular in other fields, such as uninterruptible power supplies for the telecommunications industry (Bullock, 1994).

Nickel-Cadmium (NiCd)

Nickel-cadmium (NiCd) batteries are a very mature and well-understood technology. For many years, NiCd batteries were the preferred battery type for many applications ranging from emergency medical equipment to power tools (Buchmann, 2011). However, in recent years, NiCd batteries have been largely replaced in nearly every application by emerging battery technologies such as lithium-ion (Li-ion) and nickel-metal hydride (NiMH). This is largely due to four drawbacks of NiCd batteries: low specific energy, a high self-discharge rate, and a strong presence of the memory effect. NiCd batteries are capable of providing just 40-60 W/kg, one of the lowest gravimetric energy densities of any battery, only beating out lead-acid batteries. Additionally, because Cadmium is a toxic, heavy metal, disposal of NiCd batteries is difficult and environmentally unfriendly. This negative feature of cadmium has spurred research into cleaner technologies and has led to the widespread adoption of NiMH batteries (Kularatna, 2011). NiCd battery's high self-discharge rate of 15%-25% per month means that they must be recharged after storage (Kularatna, 2011). Finally, one of the most detrimental aspects of NiCd batteries is their strong susceptibility to the "memory effect," or more correctly, the voltage depression effect (Kularatna, 2011). After being repeated partial discharges, a NiCd battery will lose its cell voltage prematurely during normal use (discharge). This often causes systems being buffered by the cell to become inoperable until a sufficient cell voltage is returned. Batteries with the voltage depression effect must be fully discharged and recharged before they will return to normal operation.

Nevertheless, NiCd batteries are not completely out of use; many features of NiCd batteries make them highly useful in niche applications (Kularatna, 2011; Buchmann, 2011). Specifically, NiCd batteries can withstand a wide range of temperatures, handling low temperatures particularly well. NiCd batteries also benefit from a very fast charge and they also have a very pronounced peak in their charging profile at 100% charge. This makes charging relatively simple when compared to NiMH batteries. Finally, NiCd batteries boast a large amount of cycle lives - up to 1000 cycles - and thus they remain the cheapest battery in terms of cost per cycle.

Nickel-Metal Hydride (NiMH)

Nickel-metal hydride batteries (NiMH) have been in use since 1989 and are still widely used thanks to an array of highly desirable features that make them ideal for many different applications (Kularatna, 2011). NiMH batteries are largely based on the Nickel-Cadmium (NiCd), however they have two important characteristics that have caused them to largely eliminate the use of their predecessor. First, they have realized about a 40% increase in specific energy over NiCd, secondly they are made of much more environmentally friendly materials and are easier to recycle (Buchmann, 2011; Fatcenko, et al., 2007).

Second, the Cadmium of NiCd batteries is replaced with a metal alloy improving the environmental friendliness of the batteries.

In addition to these characteristics, other notable features of NiMH batteries include wide range of cell sizes, safety in operation at high voltages and during charge and discharge, comparatively high energy and power densities, very low maintenance, and inexpensive charging and electronic control circuits (Fatcenko, et al., 2007).

Lithium-Ion (Li-ion)

Li-ion batteries are commonly found in consumer electronics, and are popular due to their high energy density, slow loss of charge, and minimal voltage depression effect (Buchmann, 2011). The self-discharge rate of Li-ion batteries is 5% in the first 24h after being fully charged, and then 1-2% per month. An additional 3% loss per month can be attributed to the protection circuitry that is present in nearly all Li-ion batteries. Li-ion batteries typically have specific energies between 90 and 190 Wh/kg, energy density ranging from 200 to 330 Wh/L, and a capacity range from 1 to 4 Ah.

Li-ion batteries are considered to be dangerous in some situations due to their inclusion of a flammable electrolyte and the fact that they are kept pressurized. When considering energy buffering solutions, Li-ion batteries can only be safely charged at temperatures ranging from 0°C to 45 °C. Li-ion batteries can only be safely discharged at temperatures ranging from -20°C to 60°C. Charging or discharging a Li-ion battery outside of its rated temperature limits can cause irreparable damage to the battery's capacity or can cause ruptures and leakage of electrolyte.

Li-ion batteries are of 6 main types: Lithium cobalt oxide (LCO), lithium manganese oxide (LMO), lithium iron phosphate (LFP), lithium nickel manganese cobalt oxide (NMC), lithium nickel cobalt aluminum oxide (NCA), and lithium titantate (LTO). According to Buchmann (2011), LCO has high capacity and is primarily used for cell phones, cameras and laptops. LMO, LFP, and NMC are safer have high specific power and long lifespans, but they have a lower capacity than LCO. NCA and LTO are less frequently used, but are becoming increasingly important in electric powertrains and grid storage. NCA has high specific energy and power with a long lifespan, but poor relative safety and cost. LTO batteries are extremely safe, but are rather costly and have low energy density.

Figure 6. Pictured are four supercapacitors. From left to right they are, 5 F, 50 F, 350 F, and 3000 F.

SUPERCAPACITORS

Supercapacitors, sometimes called ultracapacitors or electric double-layer capacitors (EDLCs), are electrochemical devices that represent a transition between two distinct device classes: conventional capacitors and rechargeable batteries. Supercapacitors have the highest energy density among capacitors, but are only ~10% as energy-dense as conventional batteries. What supercapacitors lack in energy density they make

up for in terms of power density. Compared to conventional batteries, supercapacitors are generally 10 to 100 times more power-dense.

Supercapacitors can derive their capacitance from two principles – the first of which is the EDL (electric double layer). The EDL is a storage structure in which charged ions from an electrolyte surface are attracted to a conductive electrode surface by electrostatic forces or selective absorption of ions into the surface (Conway, 1991). The second principle leading to energy storage in supercapacitors is pseudocapacitance, allowing chemical storage of energy, rather than electrostatic storage found in conventional batteries (Conway, 1991).

The amount of energy stored in a supercapacitor can be naïvely calculated based on its capacitance and terminal voltage. For example, taking a 2.7V, 3000F supercapacitor:

$$\mathrm{E} = \frac{1}{2}\mathrm{CV}^2 = \frac{1}{2} * 3000\ \mathrm{F} * \ 2.7\ \mathrm{V}^2 = 10{,}935\ \mathrm{J}$$

This calculation, while acceptable as a rough estimation, doesn't take into account the physics of charge storage in supercapacitors, often modeled via the commonly accepted three-branch model of super capacitors (Zubieta & Bonert, 2000). To more accurately predict the state-of-charge in a supercapacitor, a Kalman filtering approach has been used (Nadeau, Sharma, & Soyata, 2014). Assuming ideal capacitance or using a recursive calculation of stored energy yields up to 85% error in estimating state-of-charge, but by using Kalman filtering to estimate the true parameters of the three-branch model, this error can be reduced to just 1%.

When considering supercapacitors as a possible energy buffering solution, the energy harvesting method is also a key part of the decision. If solar energy is being harvested for example, cloud coverage can lead to short duration power spikes that can easily be handled by supercapacitors, but would overwhelm conventional batteries (Nadeau, Sharma, & Soyata, 2014). Supercapacitors can also be charged and discharged a greater number of times than conventional batteries, so long-term CPS installations would benefit from supercapacitors' lifespan (Buchmann, 2011).

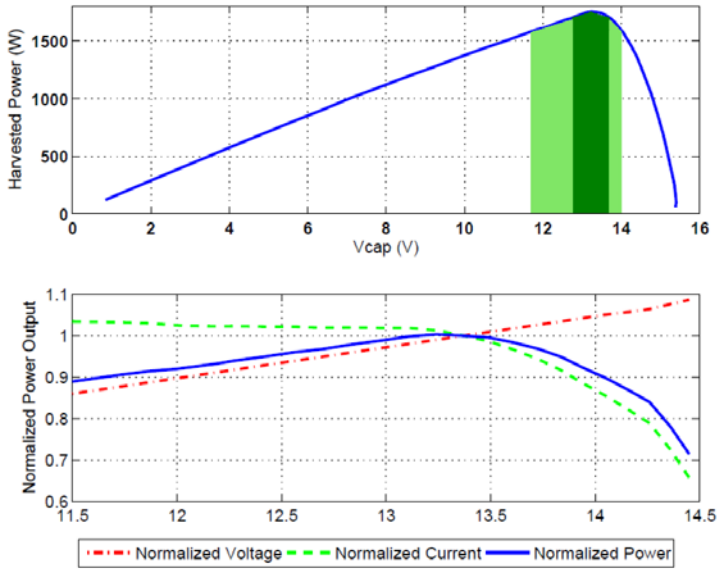

Figure 7. Non-linear I-V curve of three solar panels in series. The Maximum Power Point (MPP) is reached at 13.3V. Reprinted with permission of the authors (Hassanalieragh, Soyata, Nadeau, & Sharma, 2014).

Compared to Lithium-ion batteries, supercapacitors offer some great advantages. Given an adequate voltage, supercapacitors are capable of charging on the order of seconds (Buchmann, 2011). This superior *power* density characteristic allows supercapacitors to be used in datacenters that serve very compute-intensive applications (Page, Kocabas, Soyata, Aktas, & Couderc, 2014) (Kocabas & Soyata, 2014) (Wang,

Liu, & Soyata, 2014) (Soyata, T., Muraleedharan, R., Funai, C., Kwon, M., & Heinzelman, W., 2012) (Soyata, et al., 2012) (Kocabas, et al., 2013) (Soyata, Ba, Heinzelman, Kwon, & Shi, 2014) (Kwon, et al., 2014). Since these applications cause major spikes in power demand, supercapacitors are an excellent tool to locally store the energy and provide it to the rack computers that demand it.

Lithium-ion batteries, on the other hand, commonly take up to an hour or more to reach a full charge. Supercapacitors allow for a much greater range in charge and discharge temperature as well, between -40° and 65°C, compared to Lithium-ion batteries' range of 0-45°C for charging and -20-60°C for discharging (Buchmann, 2011). Supercapacitors' durability can also be seen in their cycle life which can reach 1 million cycles, while Lithium-ion batteries are on the order of several hundred. Supercapacitors' greatest advantage over batteries is their specific power, which can be as high as 10,000 W/kg, compared to just 3,000 W/kg for Lithium-ion batteries.

The disadvantages of supercapacitors are their low specific energy, which is usually around 5 Wh/kg, whereas Lithium-ion batteries can achieve between 100 and 200 Wh/kg (Buchmann, 2011). Additionally, they are more expensive per Watt. The price of a typical supercapacitor is around $20/Wh, while a large Lithium-ion battery can be as little as $0.50/Wh.

CYBER-PHYSICAL ENERGY HARVESTING/BUFFERING CIRCUIT DESIGN

In this section we describe the circuitry that is employed by energy sources and buffering devices. Common circuit structures to harvest energy from commonly used power sources as well as charge circuitry for energy buffering devices are provided.

Solar Energy Harvesting

When harvesting solar energy, it's important to note that a solar panel's I-V relationship is non-linear (Fahad, et al., 2012). This implies that solar panels connected in series will not yield the sum of their individual advertised power ratings. In order to use solar panels efficiently, and to yield the maximum power from solar panels, one must use a MPPT (Maximum Power Point Tracking) circuit or a software implementation to sample the output of the cells and apply the proper load resistance to ensure the solar panel is working at its maximum power point (MPP) (Femia, Petrone, Spagnuolo, & Vitelli, 2005). The MPP of a solar panel depends on the intended load, the current irradiance levels hitting the cells, and the panel's temperature (Hassanalieragh, Soyata, Nadeau, & Sharma, 2014). An example MPP curve is shown in Figure 7. An MPPT circuit or software solution simply realizes an algorithm that operates at close to the MPP of solar panels. Without MPPT circuitry/control software, solar panels can see significant degradation in efficiency.

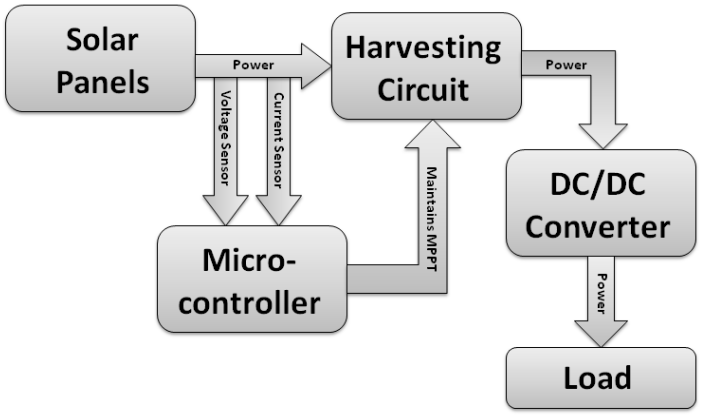

Figure 8. Block diagram of solar energy harvesting circuit (Buckley).

Two common gradient descent algorithms are used for low-cost MPPT implementation; these are Perturb and Observe (P&O) and INcremental Conductance (INC) (Femia, Petrone, Spagnuolo, & Vitelli, 2005). P&O is particularly easy to implement, but also includes some inherent oscillation around the MPP at steady state. Essentially, P&O varies the operating voltage of the PV panel in a given direction, and the power from the PV panel is observed. If the power drawn increases, this means that the operating point has become closer to the MPP, and thus the operating voltage is further perturbed in that direction until the power drawn decreases. At the point where the power drawn decreases, the operating voltage is perturbed in the opposite direction. As the perturbation approaches a very small value, and the cycle time for this algorithm decreases, the problem of oscillating around the MPP is reduced but never fully eliminated.

INC attempts to solve the oscillation problem, but is algorithmically more complex, which translates to slower sampling rates and increased cost in terms of power and hardware. INC is based on the observation that at MPP, $di_{PV}/dv_{PV} + i_{PV}/v_{PV} = 0$, where i_{PV} is the PV panel current and v_{PV} is the PV panel's voltage (Femia, Petrone, Spagnuolo, & Vitelli, 2005).

If $di_{PV}/dv_{PV} + i_{PV}/v_{PV} < 0$, this means the operating point is to the right of the MPP on the V-P plane, and if $di_{PV}/dv_{PV} + i_{PV}/v_{PV} > 0$, this means the operating point is to the left of the MPP. INC causes a perturbation in the correct direction based on the sign of the quantity $di_{PV}/dv_{PV} + i_{PV}/v_{PV}$, and when the quantity = 0 within a reasonable tolerance, the algorithm stops all perturbation to prevent the oscillation problem.

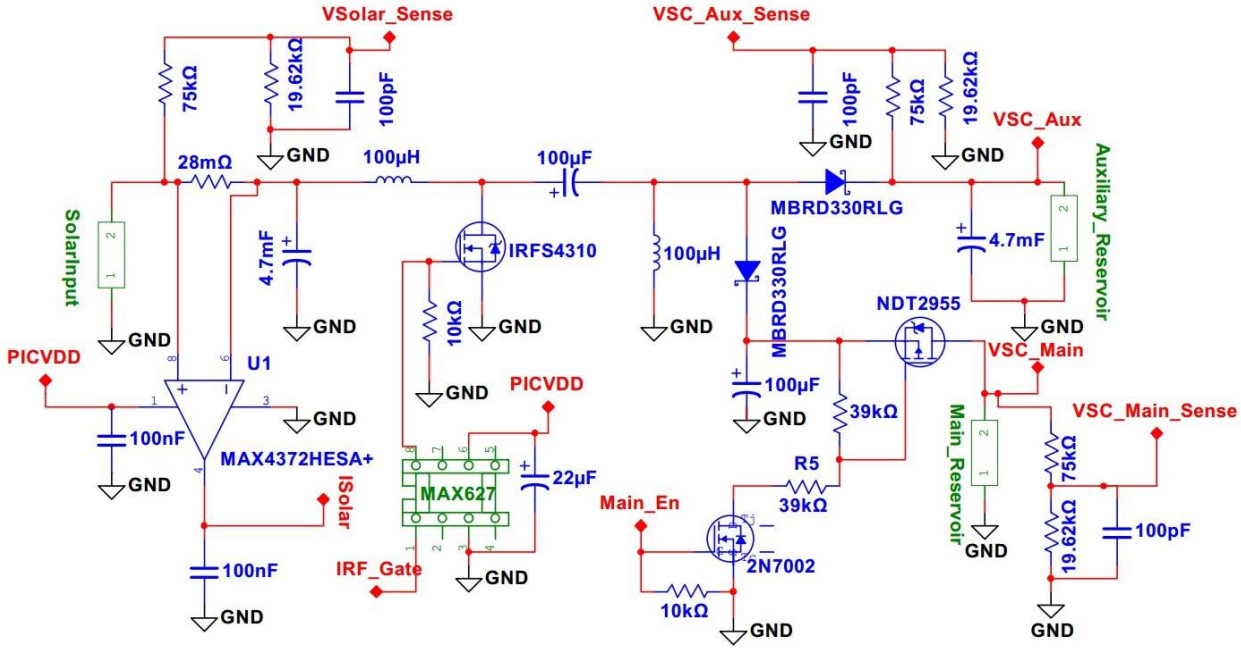

Figure 9. Solar Energy Harvesting Circuit built around a SEPIC DC-DC converter. Reproduced with permission of the authors (Hassanalieragh, Soyata, Nadeau, & Sharma, 2014).

Figure 8 shows one way to design a simple P&O or INC circuit. A major issue with both P&O and INC is that they may are not well-suited to determine local versus global maximums and minimums, and thus may be stuck at a local optimum operating point. A third and final algorithm that is relatively simple to implement and solves this local optimum problem is the fractional open circuit voltage method. This

method approximates the MPP as a fraction of the open circuit voltage, usually around 75%, but this differs based on environmental conditions (Ahmad, 2010). In this method, a measurement is made of the open circuit voltage, and then the circuit attempts to keep the input solar power at 75% (or whatever fraction is correct for the environmental conditions) of that measurement. There are still draw backs with the fractional open circuit method: the method is approximate rather than exact; also, to measure the open circuit voltage, harvesting must be stopped for a small duration of time.

Energy Storage with Supercapacitors

Supercapacitors are very easy to charge as they do not require any specific circuitry that ensures a specific charging pattern; simply applying a terminal voltage that causes current to flow into the supercapacitor allows it to store energy. Depending on the source of the input energy, circuitry may be required to ensure energy is being transferred efficiently. As an example, Figure 9 depicts circuitry used to buffer energy from solar panels.

The most important function of the circuitry shown in Figure 9 is to ensure that the solar panel input is kept at the MPP. The circuit in Figure 9 achieves this goal through the use of a SEPIC DC-DC converter (Hassanalieragh, Soyata, Nadeau, & Sharma, 2014). After measuring the voltage of the attached solar panels, a switch adjusts the duty cycle for the circuit, thus increasing or decreasing the average current demanded from the solar panels. As the duty cycle increases, there is increased average current demand from the solar panel due to the leftmost inductor in the SEPIC configuration. As this inductor is turned on for a greater percentage of time, more power is demanded, and the less time it's on, average current demand decreases. This allows the I-V curve of the solar panel to be adjusted, thus maintaining the optimum point for harvesting maximum power.

The SEPIC DC-DC converter is used for the following reasons (Hassanalieragh, Soyata, Nadeau, & Sharma, 2014): firstly, SEPIC is capable of both up-converting and down-converting, whereas boost and buck designs can only do one or the other; secondly, the SEPIC has a continuous-input and discontinuous-output current draw. This implies that at high frequencies, capacity losses at the supercapacitor block can be eliminated with the proper electrolytic capacitors on the output side of the system. And third, since this system is meant to operate in the field in a variety of harsh environmental conditions, having a graceful short-circuit response of SEPIC is invaluable.

Current sensing is a vital part of MPPT and is generally done through a small resistor called a sense resistor, typically in the range of 5-100 mΩ. Because the voltage drop across the sense resistor is so small, the circuit shown in Figure 9 includes a current sense amplifier to amplify the voltage before it's sent to the ADC of a microcontroller. The correct current sense amplifier for a circuit depends on the amplifiers placement within the circuit. High side sensing, in which the sense resistor is placed directly after the input source, requires a different current sense amplifier than low side sensing because the sense resistor will be subjected to high common mode voltage. The circuit in Figure 9 uses a MAX4372H, which

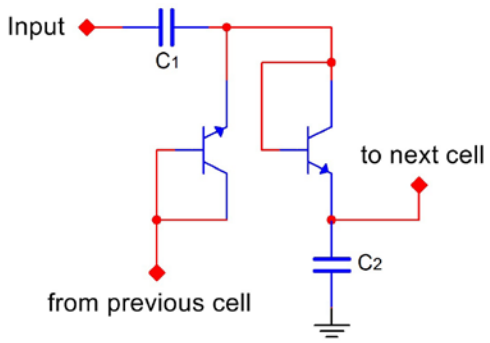

Figure 10. Charge pump circuit that might be found in an RF harvesting system Based on Shameli, Safarian, Rofougaran, Rofougaran, & De Flaviis, 2007.

is a high side current sense amplifier. A final consideration when choosing current sense amplifiers is their intended use for measuring DC current. Because current sense amplifiers are designed for DC current their effective bandwidth is not high (Hassanalieragh, Soyata, Nadeau, & Sharma, 2014).

When working with supercapacitors one should also be aware of the variable manufacturing tolerances. Due to these manufacturing tolerances, supercapacitors can easily be overcharged when there are multiple supercapacitors arranged in series. For example, among eight supercapacitors rated to be 3000 F, researchers at the University of Rochester measured actual capacitances ranging from 2855 F to 3139 F. In this situation, charging the eight supercapacitors as a block to the theoretical maximum of 21.6 V would overcharge the smaller supercapactiors beyond their maximum of 2.7 V. This is because the same current flowing through each would charge the smallest supercapacitor (2855 F) to 2.87 and the largest supercapacitor (3139 F) to only 2.61 V. Although complicated circuitry could be implemented to control the charging of each supercapacitor individually, the simplest solution is to charge the supercapacitor block to a voltage below its rated maximum. This leads to inefficient use of the larger supercapacitors; for Hassanalieragh et al., this technique yielded a total voltage of 20.3 V, or 94% efficiency.

RF Energy Harvesting

In a system designed to utilize RF energy, such as an RFID device, the power harvester has two important functions: rectifying the receiving signal and generating the supply voltage (Shameli, Safarian, Rofougaran, Rofougaran, & De Flaviis, 2007). The power harvesting circuitry consists of a series of rectifier cells, similar to the one shown in Figure 10 with each cell building on the voltage of the one before it, in order to accumulate the supply voltage.

This functionality is commonly achieved through a charge pump. The circuit in Figure 10 shows a series of rectifier cells, each consisting of a DC-level shifter and a peak detector. In the first half of the signal's period when voltage is low, the sampling capacitor C_1 will be charged up to a certain level depending on the amplitude of the input signal, the voltage drop across the diode, and the voltage of the cell preceding it in the chain.

In order to maximize the efficiency of the harvesting circuitry, the voltage drop across the diode must be minimized. A simple and frequently suggested solution is to use high efficiency Schottky diodes, but such diodes are not available in standard CMOS processes, and therefore would need to be specially manufactured, greatly increasing the cost of the circuit (Jabbar, Song, & Jeong, 2010; Shameli, Safarian, Rofougaran, Rofougaran, & De Flaviis, 2007). Therefore, a method of reducing voltage losses which is available in standard CMOS processes is highly desirable.

Currently, no way exists to increase the efficiency of the diodes using standard CMOS processes that yields efficiency comparable to Schottky diodes at very low voltage levels; however, a passive network used to increase the amplitude of the input signal at the input of the charge-pump circuit can mitigate some of

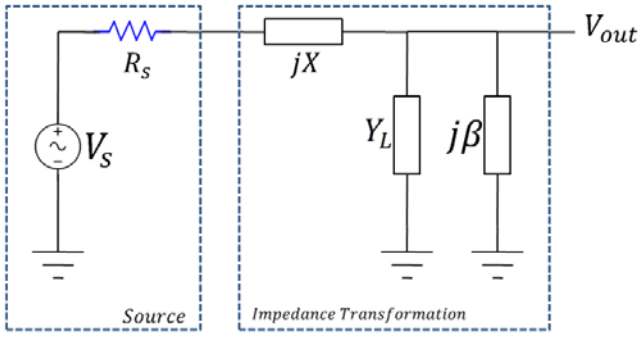

Figure 11. Impedance transformation circuit Based on Shameli, Safarian, Rofougaran, Rofougaran, & De Flaviis, 2007.

the challenges of operating at very low voltage levels (Shameli, Safarian, Rofougaran, Rofougaran, & De Flaviis, 2007).

Because the circuit is so sensitive to low voltages, voltage losses in the circuit must be minimal in order to achieve relatively high efficiency with the power harvester. One way to minimize losses is through an impedance matching circuit as shown in Figure 11. This circuit matches the load impedance to the input impedance, which results in the ideal conditions for power transfer from the source to the load. In order to achieve the greatest possible output voltage, the input impedance should be equal to the source impedance.

Charge Circuitry for Rechargeable Batteries

Charge circuitry for NiCd batteries relies on full-charge detection based on either temperature or voltage signature (Buchmann, 2011). Low-cost charging circuitry simply measures the external surface temperature of the battery and compares the measurement to a known cut-off value (Buchmann, 2011). Most low cost NiCd chargers use 50 °C as this cut-off temperature, at which point the charger turns on its "ready" light to indicate full-charge. Temperatures exceeding 45 °C can damage NiCd cells, but brief exposure to 50 °C to detect a full charge is standard. Higher cost temperature based chargers involve using a microcontroller to measure the rate dT/dt of temperature change. Charging is stopped upon detecting a high rate of temperature increase characteristic of the end of a charge cycle. Charger manufacturers commonly use 1°C per minute as the cut-off rate, but if the battery's dT/dt never reaches this rate, maximum temperature based shut-off is also in place to prevent charging after the battery reaches 60°C. Temperature-based full-charge detection isn't ideal because when a fully charged battery is inserted into a charger it becomes overcharged, thus damaging the battery.

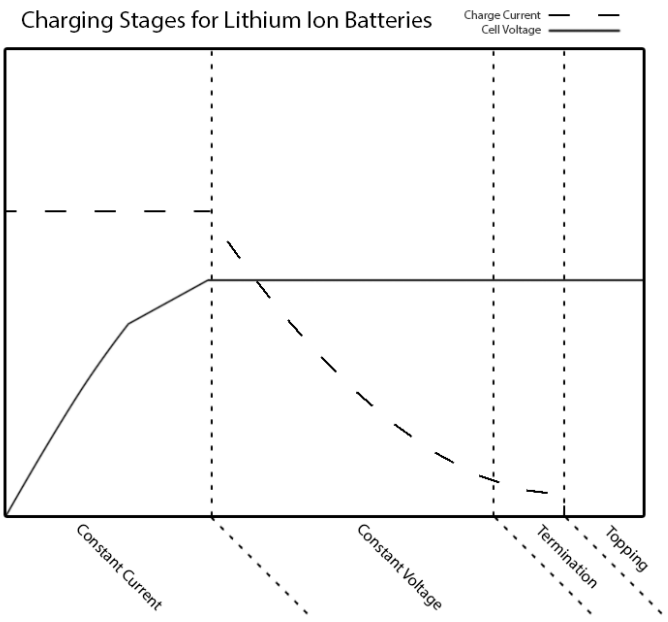

Figure 12. Charging stages for lithium-ion batteries.

A more advanced method of full-charge detection is via voltage signature. A microcontroller can be used to poll for voltages and compare recent values to detect a specified voltage signature. Once the microcontroller detects the end of a charge cycle via a characteristic voltage drop, or negative delta V (NDV), charging stops. NDV detection typically looks for a drop of 10mV per cell to indicate full-charge, but this method requires a charge rate of 0.5C or higher. The C-rate here is a measure of the rate at which a battery is charged or discharged relative to its maximum capacity. For example, a 1C rate means that a 1.0Ah battery would be discharged in one hour at a discharge rate of 1.0A, or at 0.5C the same battery would provide 500mA for two hours. In addition to NDV detection, charging microcontrollers also include plateau detection that stops charging after the voltage has been stuck in a steady state.

Charging of NiMH batteries relies on the same principles, but NDV detection is much more subtle for NiMH batteries. The voltage drop at the end of a charge cycle is only 5mV, so NiMH chargers use electronic filtering to provide a clean signal to the microcontroller. A combination of many detection methods is common in modern chargers, including NDV, voltage plateau, dT/dt, absolute temperature, and timers – whichever method triggers first is used to shut off the charging.

Charging lead acid batteries is very slow compared to other rechargeable batteries. A sealed lead acid battery takes 12-16 hours to charge, but for large stationary batteries, it can take up to 48 hours. This time can be reduced to 10 hours or less with special charging methods, but these aren't as precisely characterized and the battery may not be fully charged as a result. The method used in charging lead acid batteries involves three distinct phases, the first of which is a constant-current phase which takes about half of the charging time and provides most of the final charge. The second stage is the topping phase, which continues at a lower constant current and saturates the cell. Finally the float charge stage recharges the battery, as needed, due to self-discharge.

Stage one brings the cell charge to 70% and takes 5-8 hours, and in the next 7-10 hours stage two brings the battery up to 100%. The transition between stage one and two occurs when the battery has reached a set voltage limit. Full charge is considered reached when the current drops to 3% of the rated current for the battery. If the battery doesn't reach this low saturation current, a plateau timer is used to stop charging. The float charging phase is merely present to keep the battery fully charged as it slowly self-discharges.

Li-on batteries are charged in a manner similar to lead acid batteries, and the charging pattern is illustrated in Figure 12. The major differences between Li-ion charging and lead acid charging are that (1) Li-ion cells are higher voltage than their lead acid counterparts, (2) Li-ion charging must be more precise because Li-ion batteries have much less tolerance for overcharging, and (3) Li-ion charging doesn't include a float charging phase. Most Li-ion cells charge to 4.2V with a tolerance of around 50mV; overshooting this tolerance is unsafe and will most likely damage the battery.

The constant current phase of charging for Li-ion cells has a rate of around 1C and this takes around three hours. The charging then transitions into phase two where the cell is kept at a constant voltage. Charging stops when the current reaches 3% of the rated maximum for the cell, and then finally topping charging occurs as needed. High current can be used to rapidly reach 70% charge, but the topping phase will take longer. Using only 70% of the battery's capacity is recommended unless the full capacity is truly required. Fully charging a Li-ion battery reduces the battery's ability to fully charge again.

Sample Use Cases for CPS

In this section we survey a few examples of energy sources and buffering mechanisms commonly used in cyber physical systems. ZebraNet (Philo Juang, 2002) is a mobile sensor network primarily indented to collect data and study the biological behavior of zebras in central Kenya. Zebranet is an example of a CPS used for wildlife monitoring and analysis. Each ZebraNet node contains a GPS system with user-programmable CPU, non-volatile memory storage for data logging and radio transceivers for data communication. Based on the nature and location constraints of the application, solar cells are used as the energy source of the system and rechargeable Lithium-Ion Batteries are employed for energy buffering.

Everlast (Simjee & Chou, 2006) in another example of a CPS that is powered by solar energy. Each Everlast node contains a light sensor and an accelerometer bundled with a low power microprocessor and a wireless transceiver. Since extended unsupervised operation (20 years without maintenance) is a

primary goal in Everlast, the system uses supercapacitors as the only energy buffering mechanism. On the sensing part, Everlast contains a light sensor with a pin-selectable light aperture for measuring a wide dynamic range of light intensity and an ultra low power dual accelerometer consuming 600 uA.

A wireless sensor node for distributed active vibration control (AVC) in automotive applications has been proposed by (Zielinski, Mieyeville, Navarro, & Bareille, 2014). The piezoelectric element in the system turns vibrations into electrical energy to power up the storage, conversion and processing units. The work proposed in (Parks, Sample, Zhao, & Smith, 2013) is an example of a wireless sensor node utilizing ambient RF energy to power up an entire sensing, processing, and communication system. The energy harvesting part consists of an antenna, impedance matching and a charge pump for converting the RF energy into electrical energy. The application platform includes on board sensors for gathering information, a microcontroller and a 2.4 GHz radio. While the implementation used a ceramic chip capacitor, the authors do point out that the use of rechargeable batteries and high density supercapacitors can increase the system life time to 10 - 20 years, albeit with increased system complexity and cost.

Exploiting multiple energy sources and a hybrid energy buffering mechanism has been proposed as a solution to increase the reliability and longevity of operation in CPS. For example, AmbiMax (Park & Chou, 2006) is an autonomous energy harvesting platform using solar and wind energy and a hybrid architecture of supercapacitors and Lithium Polymer batteries to sustain the operation of an Eco wireless sensor node (Park C. a., 2005). Eco is an ultra-compact wireless sensor node for real-time motion monitoring that combines a two-axis accelerometer and 2.4 GHz GFSK radio for data transmission.

CPSs that require long-term maintenance-free operation are increasingly moving toward supercapacitor based energy buffering because of the advantages supercapacitors offer over batteries. Also, because of the relative simplicity of supercapacitors energy modeling, these devices are also an attractive choice for intelligent CPSs, where precise energy management and control is essential.

ACKNOWLEDGMENT

This work was supported in part by the National Science Foundation grant CNS-1239423 and a gift from Nvidia Corp.

REFERENCES

Ahmad, J. (2010). A Fractional Open Circuit Voltage Based Maximum Power Point Tracker for Photovoltaic Arrays. *Software Technology and Engineering (ICSTE), 2010 2nd International Conference on (Vol 1)* (pp. V1-247 - V1-2250). San Juan, Puerto Rico: IEEE.

Andrewatla. (2007, September 19). *Solar panel.* Retrieved August 27, 2014, from freeimages: http://www.freeimages.com/photo/873825

Atwood, B., Warneke, B., & Pister, K. S. (2000). Preliminary Circuits for Smart Dust. *Mixed-Signal Design, 2000. SSMSD. 2000 Southwest Symposium on* (pp. 87-92). San Diego, California: IEEE.

Beeby, S. P., Tudor, M. J., & White, N. M. (2006). Energy harvesting vibration sources for microsystems applications. *Measurement Science and Technology,* R175-R195.

Buchmann, I. (2011). *Batteries in a Portable World.* Vancouver, Canada: Cadex Electronics Inc.

Buckley, B. (n.d.). *MPPT- Maximum Power Point Tracking.* Retrieved from Bryan Buckley: http://bryanwbuckley.com/projects/mppt.html

Bullock, K. R. (1994). Lead/acid batteries. *Journal of Power Sources*, 1-17.

Chalasani, S., & Conrad, J. M. (2008). A Survey of Energy Harvesting Sources for Embedded Systems . *Southeastcon, 2008. IEEE* (pp. 442-447). Huntsville, Alabama: IEEE.

Conway, B. E. (1991). Transition from "Supercapacitor" to "Battery" Behavior in Electrochemical Energy Storage. *Journal of The Electrochemical Society*, 1539-1548.

Curty, J.-P., Joehl, N., Dehollain, C., & Declercq, M. J. (2005). Remotely Powered Addressable UHF RFID Integrated System. *IEEE Journal of Solid-State Circuits*, 2193-2202.

DebbieMous. (2011, September 16). *Solar panels reflecting the sky.* Retrieved August 27, 2014, from freeimages: http://www.freeimages.com/photo/1364625

Fahad, A., Soyata, T., Wang, T., Sharma, G., Heinzelman, W., & Shen, K. (2012). SOLARCAP: Super Capacitor Buffering of Solar Energy for Self-Sustainable Field Systems. *Proceedings of the 25th IEEE International System-on-Chip Conference (IEEE SOCC)* (pp. 236-241). Niagara Falls, New York: IEEE.

Fatcenko, M., Ovshinsky, S., Reichman, B., Young, K., Fierro, C., Koch, J., . . . Ouchi, T. (2007). Recent Advances in NiMH battery technology. *Journal of Power Sources*, 544-551.

Feldman, D., Barbose, G., Margolis, R., Darghouth, N., & Goodrich, A. (2012). *Photovoltaic (PV) Pricing Trends: Historical, Recent, and Near-Term Projections.* Golden, Colorodo: National Renewable Energy Laboratory.

Femia, N., Petrone, G., Spagnuolo, G., & Vitelli, M. (2005). Optimization of Perturb and Observe Maximum Power Point Tracking Method. *IEEE Transactions on Power Electronics*, 963-973.

Foster, K., & Jaeger, J. (2007). RFID Inside. *IEEE Spectrum*, 24-29.

Goudarzi, N., & Zhu, W. (2013). A review on the development of wind turbine generators across the world. *International Journal of Dynamics and Control*, 192-202.

Green, M. A., Emergy, K., Hishikawa, Y., Warta, W., & Dunlop, E. D. (2014). Solar cell efficiency tables (version 44). *Progress in Photovoltaics: Research and Applications*, 701-710.

Guigon, R., Chaillout, J.-J., Jager, T., & Despesee, G. (2008a). Harvesting raindrop energy: theory. *Smart Materials and Structures*, 25-39.

Guigon, R., Chaillout, J.-J., Jager, T., & Despesse, G. (2008b). Harvesting raindrop energy: experimental study. *Smart Materials and Structures*, 15-39.

Hande, A., Polk, T., Walker, W., & Bhatia, D. (2007). Indoor solar energy harvesting for sensor network router nodes. *Microprocessors and Microsystems*, 420-432.

Hassanalieragh, M., Soyata, T., Nadeau, A., & Sharma, G. (2014). Solar-Supercapacitor Harvesting System Design for Energy-Aware Applications. *Proceedings of the 27th IEEE International System-On-Chip Conference (IEEE SOCC 2014).* Las Vegas, Nevada: IEEE.

Hudak, N. S., & Amatucci, G. G. (2008). Small-scale energy harvesting through thermoelectric, vibration, and radiofrequency power conversion. *Journal of Applied Physics*, 101301.

Jabbar, H., Song, Y. S., & Jeong, T. T. (2010). RF Energy Harvesting System and Circuits for Charging Mobile Devices. *IEEE Transactions on Consumer Electronics*, 247-253.

Kahn, J. M., Katz, R. H., & Pister, K. S. (2000). Emerging challenges: Mobile networking for "Smart Dust". *Journal of Communications and Networks*, 188-196.

Kocabas, O., & Soyata, T. (2014). Medical Data Analytics in the Cloud Using Homomorphic Encryption. In P. Chelliah, & G. Deka, *Handbook of Research on Cloud Infrastructures for Big Data Analytics* (pp. 471-488). IGI Global.

Kocabas, O., Soyata, T., Couderc, J., Aktas, M., Xia, J., & Huang, M. (2013). Assessment of cloud-based health monitoring using Homomorphic Encryption. *Proceedings of the 31st IEEE International Conference on Computer Design*, (pp. 443-446). Asheville, NC.

Kularatna, N. (2011). Rechargeable Batteries and Their Management. *IEEE Instrumentation and Measurement Magazine*, 20-33.

Kwon, M., Dou, Z., Heinzelman, W., Soyata, T., Ba, H., & Shi, J. (2014). Use of Network Latency Profiling and Redundancy for Cloud Server Selection. *Proceedings of the 7th IEEE International Conference on Cloud Computing*, (pp. 826-832). Alaska.

Mi, M., Mickle, M. H., Capelli, C., & Swift, H. (2005). RF Energy Harvesting with Multiple Antennas in the Same Space . *IEEE Antennas and Propagation Magazine*, 100-106.

Myers, R., Vickers, M., Kim, H., & Priya, S. (2007). Small scale windmill. *Journal of Applied Physics*, 054106.

Nadeau, A., Sharma, G., & Soyata, T. (2014). State-of-Charge Estimation for Supercapacitors: A Kalman Filtering Approach. *Proceedings of the 2014 IEEE International Conference on Acoustics, Speech and Signal Processing (ICASSP 2014)* (pp. 2213-2217). Florence, Italy: IEEE.

Ohya, Y., Karasudani, T., Sakurai, A., Abe, K.-i., & Inoue, M. (2008). Development of a shrouded wind turbine with a flanged diffuser. *Journal of Wind Engineering and Industrial Aerodynamics*, 524-539.

Page, A., Kocabas, O., Soyata, T., Aktas, M., & Couderc, J. (2014). Cloud-Based Privacy-Preserving Remote ECG Monitoring and Surveillance. *Annals of Noninvasive Electrocardiology (ANEC)*.

Park, C. a. (2005). Eco: an Ultra-Compact Low-Power Wireless Sensor Node for Real-Time Motion Monitoring. *Proceedings of the 4th International Symposium on Information Processing in Sensor Networks*. Los Angeles, CA: IEEE Press.

Park, C., & Chou, P. (2006). AmbiMax: Autonomous Energy Harvesting Platform for Multi-Supply Wireless Sensor Nodes. *Sensor and Ad Hoc Communications and Networks, 2006. SECON '06. 2006 3rd Annual IEEE Communications Society on* (pp. 168,177). Reston, VA: IEEE.

Parks, A. N., Sample, A. P., Zhao, Y., & Smith, J. R. (2013). A wireless sensing platform utilizing ambient RF. *Topical Conference on Wireless Sensors and Sensor* (pp. 127-129). IEEE.

Philo Juang, H. O.-S. (2002). Energy-Efficient Computing for Wildlife Tracking:Design Trade-Offs and Early Experiences with ZebraNet. *Proceedings of the 10th international conference on Architectural support for programming languages and operating systems*. San Jose, CA.

Randall, J. F., & Jacot, J. (2002). The performance and modelling of 8 Photovoltaic materials under variable light intensity and spectra. *World Renewable Energy Congress VII & Expo*. Cologne, Germany.

Roundy, S., Steingart, D., Frechette, L., Wright, P., & Rabaey, J. (2004). Power Sources for Wireless Sensor Networks. In H. Karl, A. Wolisz, & A. Wilig, *Wireless Sensor Networks* (pp. 1-17). Berlin: Springer Berlin Heidelberg.

Shad, R., Wright, P. K., & Pister, K. S. (2002). Micro-Electrostatic Vibration-to-Electricity Converters. *Proceedings of IMECE2002*. New Orleans, Lousiana: ASME.

Shameli, A., Safarian, A., Rofougaran, A., Rofougaran, M., & De Flaviis, F. (2007). Power Harvester Design for Passive UHF RFID Tag Using a Voltage Boosting Technique. *IEEE Transactions on Microwave Theory and Techniques*, 1089-1097.

Simjee, F., & Chou, P. (2006). Everlast: Long-life, Supercapacitor-operated Wireless Sensor Node. *Low Power Electronics and Design, ISLPED'06* (pp. 197,202). Tegernsee: IEEE.

Soyata, T., Ba, H., Heinzelman, W., Kwon, M., & Shi, J. (2014). Accelerating Mobile-Cloud Computing: A Survey. In *Communication Infrastructures for Cloud Computing* (pp. 175-197). IGI Global.

Soyata, T., Muraleedharan, R., Ames, S., Langdon, J., Funai, C., Kwon, M., & Heinzelman, W. (2012). COMBAT: mobile-Cloud-based cOmpute/coMmunications infrastructure for BATtlefield applications. *Proceedings of SPIE*, (pp. 84030K-13). Baltimore, MD.

Soyata, T., Muraleedharan, R., Funai, C., Kwon, M., & Heinzelman, W. (2012). Cloud-Vision: Real-time face recognition using a mobile-cloudlet-cloud acceleration architecture. *Symposium on Computers and Communications (ISCC)* (pp. 59-66). IEEE.

Thomas, J. P., Qidawi, M. A., & Kellogg, J. C. (2006). Energy scavenging for small-scale unmanned systems. *Journal of Power Sources*, 1494-1509.

Visser, H. J., & Vullers, R. J. (2013). RF Energy Harvesting and Transport for Wireless Sensor Network Applications: Principles and Requirements. *Proceedings of the IEEE*, 1410-1423.

Wang, H., Liu, W., & Soyata, T. (2014). Accessing Big Data in the Cloud Using Mobile Devices. In P. Chelliah, & G. Deka, *Handbook of Research on Cloud Infrastructures for Big Data Analytics* (pp. 444-470). IGI Global.

Wang, L., & Yuan, F. G. (2007). Energy harvesting by magnetostrictive material (MsM) for powering wireless sensors in SHM. *Sensors and Smart Structures Technologies for Civil, Mechanical, and Aerospace Systems 2007.* San Diego, California: SPIE.

Zielinski, M., Mieyeville, F., Navarro, D., & Bareille, O. (2014). A low power wireless sensor node with vibration sensing and energy harvesting capability. *A low power wireless sensor node with vibration sensing and energy harvesting capability* (pp. 1065,1071). Warsaw: IEEE.

Zubieta, L., & Bonert, R. (2000). Characterization of double-layer capacitors for power electronics. *IEEE Transactions on Industry Applications*, 199-205.